BJES Basrah Journal for Engineering Sciences

Basrah Journal for Engineering Sciences, Vol. 25, No. 2, (2025), 50-60

Original Article

Journal homepage: https://bjes.edu.iq/bjes
ISSN (Online): 23118385, ISSN (Print): 18146120

Experimental and Computational Analysis of Slug Flow Through a Horizontal Perforated Wellbore

Ahmed Hatif Kareem [1]*, Qais A. Rishack [2], Mohammed A. Abdulwahid [3]

[1,2] *Department of Mechanical Engineering, College of Engineering, University of Basrah, Basrah, Iraq*
[3] *Thermal Mechanical Engineering Department, Basrah Engineering Technical College, Southern Technical University, Basrah, Iraq*
E-mail addresses: engpg.ahmed.hatif@uobasrah.edu.iq , qais.rashck@uobasrah.edu.iq , mohw2016@stu.edu.iq

Article Info

Article history:
Received: 2 August 2025
Revised: 25 August 2025
Accepted: 9 September 2025
Published: 31 December 2025

Keywords:
Horizontal wellbore,
Perforation,
Mixing effect,
Pressure drop.

https://doi.org/10.33971/bjes.25.2.6

Abstract

There have been efforts and studies that have been carried out with respect to the flow patterns, pressure drops (PD), and void fraction (VF) that can be found in horizontal wells. Notwithstanding, particular attention has not been paid to research of two-phase flow (TFF) in perforated horizontal boreholes. Recently, a number of attempts have been undertaken to investigate the features of gas-liquid systems, which exist in a TFF in a perforated horizontal wellbore, which is a little studied tree of the wellbore family. The stated investigations are devoted to the TFF of liquid and gas in a horizontal wellbore, which has a diameter and length of 25.4 mm × 3 m respectively, with 18 uniform perforations. In the developed Fluent VOF model integrated in ANSYS 22 R1, the turbulence treatment and flow conditions within three-dimensional space, including water and air, with various flow rates were used to study the influence of high water and air velocities (SVW, SVA) on flow characteristics including PD, production (Q), VF, and liquid retention time in a horizontal well. The sequences of slug flow (SF) phenomena have been studied in detail for this pulsated flow. In particular, the first scenario is where SVW can reach velocities of 1.22 m/s and SVA of 1.68 m/s; in the second scenario, an increase in the SVW to 2.52 m/s is noted; and in the last scenario, the value of SVA is increased to 2.2 m/s. The empirical study was mainly targeted on the SF through a perforated horizontal wellbore. The productivity (Q), PD, and SF were found to benefit from an increase in axial flow rate (SVW), more than from increase in radial flow rate (SVA). In scenario two, productivity rises by even 84.108% as SVW changes, while in the last scenario Q increases by only 9.708% as SVA is increased. Further, the numerical and experimental results provide a reasonable match.

1. Introduction

Towards the end of the 20th century, technology for horizontal wells transformed the petroleum industry. Artificially bent or vertical wells have smaller contact areas, while order of the day are constructions of horizontal wells which are best in segmentation of large reservoirs into many layers. Horizontal wells continue to be the basic method of drilling of oil and gas. With the ability to enhance oil production by expediting the horizontal drilling process, it has as a result dominated the vertical drilling process in contemporary activities in the extraction of crude oil. Horizontal wellbore drilling is said to be more expensive than the vertical form of the same. Conventional drilling techniques are not suitable for drilling horizontal wellbore perforations; therefore, equipment of different types and designs is required to be available at the site and/or within the tooling storage. Production performance of horizontal wellbore depends on several factors including the flow patterns resulting from change in multiphase flow rate inside the wellbore.

Kim et al. [1] Due to the decrease in pressure in the horizontal wellbore, these tendencies had to negatively influence output. The target of that investigation and restatement is as follows: to determine what the features of perforated horizontal wellbore systems are, which could be subject to specific flow regimes: which regimes are favorable for production and which ones are not. Slug flow is ever present in many processes, among them, oil-gas pipe lines and heat exchangers used in power plants. This flow regime is distinguished by elongated bubbles (ELB) and liquid slugs (SF) relative to one another, with each slug containing a small gas bubble (BF). As the slug flow (SF) is not continuous, it generates great transient disturbances along the direction of flow resulting into considerable pressure fluctuations in the whole pipeline system comprising of pipes, supports, and gas/oil separators and so on, leading to mechanical shaking of the whole system. Such vibrations can also lead to damage of the full length of the pipeline system as these vibrations can exert abnormal structural stresses on the system. In order to overcome these problems, experiments and models have been used with respect to properties of the two-phase flow (TFF) SF which vary due to different geometric parameters and operating conditions.

Heck et al. [2] have gone further to provide either full analytical or a partial mechanistic approach to modeling the bottom frictional losses (F) in TFF systems based on an experimental approach. Researchers who need to predict macroscopic F, pressure drop (PD) during two-phase gas liquid flow often resort to the correlations proposed.

Shannak [3] The classic correlations are based upon two extensive collections of points PD data containing first 25, 000 points of PD data and later 9, 300 points of PD data. It attempts made provide the readers with averages of two-

phase frictional pressure drop correlations including wide ranges of working fluids and configuration of the channel widths. Taitel et al. [4] Considering the work of SF presents the most complicated and the most unstable flow forms. The SF has dominated the research on horizontal pipes.

Abdul-Majeed et al. [5] The three-dimensional airflow and water flow are modeled with ANSYS CFX-5.7 using the VOF of Homogeneous Phase. The developed CFD model accurately predicts when slugs would induce flow into and propagate within a horizontal circular pipe. The bond of slug body and liquid film is essentially resources spent in momentum transfer. The SF retention of a TFF, either slightly sloping or nearly horizontal, has been reported later using a regression method. To keep the slugs more stable, it was altered the viscosity of the liquid, roller angle and mixing speed. In oil and gas industry it is a common practice to perforate pipelines and casing to complete horizontal wells. It is common practice to perform horizontal drilling and selective completion in wells with several zones and high productivity contrast to avoid collapse of unstable formations, reduce well cost, and delay early gas or water breakthrough. Yildiz [6] used an improved nonlinear regression model to predict slug liquid holdup in the horizontal pipeline.

Banerjee et al. [7] in a number of industrial applications, SF, which occurs when the volumetric flow rates (Q) of gas and liquid are equal, is very useful. Among such activities are drilling of wells for oil, gas extraction and transportation of this fluid via pipelines, the use of pipelines to handle and transport cryogenic fluids, steam turbine power plants, and emergency cooling of nuclear plants. Abdulwahid et al. [8] have done a study performed a computational study of air and water SF through horizontal and vertical pipes with elbows. One can also perform simulation and find an effect of void fraction (VF), liquid holdup (LH), and liquid film thickness on PD through cutting.

Azadi et al. [9] perforating retains the wellbore to an extent and prevents productive wells from caving after being drugged. Dukler et al. [10] observe that SL, LH, and frequency (FR) can be modeled with the horizontal flow model. Up to now, several studies addressing central problem have noted the measures of PD in a perforated wellbore as the sum of FR, acceleration (ACC), perforation pore pressure, and mixing. Most studies are focused on the PD oscillations related to ACC and viscous friction (VIF) along the horizontal wellbore. Very few studies have been conducted investigating the TFF of pressurized water and air due to the perforations of the wellbore. Hua et al. [11] it was a revision of the PD model which involved horizontal PD inside the wellbore where mass flow inside the wellbore was included.

Wen et al. [12] it was established that three types were most significant and caused most of total PD, these were mixing, ACC and VIF. With regards to PD in horizontal wellbore, fluid viscosity plays more significant role on overall pressure and frictional pressure than on ACC and mixing PD. One may also say that both effects are PD viz structure effect of the liquid increases its viscosity used numerical and experimental methods to research horizontal wells. With the increase in the AXF of the perforating gun, there was an increase in the PD during perforation not only in single phase system but also in TFF systems although RDF remained the same. While the aggregate flow rate remains constant, it increased in relation to the main pipe flow ratio.

Landman [13] setup for the experiments measured how the type of fluid and the manner by which the hole is opened affect the pressure developed within a horizontal gas well with liquid retention at specified levels. With the increase in the number of clusters and the increase in perforation input, the pressure around each cluster increased. It does not matter if the existing holes are of uniform distribution or otherwise when adding up the total pressure drop (TPD). What happens is that the pressure at the original perforation remains almost constant when the amount of LH is greater than 0.5 but quickly increases when this fraction is lower than 0.5. Many research addressed slug flow patterns (SFP) has not been paid regarding pressure reduction in horizontal perforated wellbore dominantly.

In this CFD analysis with three different wellbore cross sections, the effect of increased axial and RDF on PD, productivity and the effect on the distribution of volume fraction (VF) in several horizontal wellbore cross sections is analyzed. This document compares three particular cases with experimental data that demonstrate the behavior of SF down a horizontal wellbore. This article elucidates the effects of distribution perforation density (DPD) in detail. Analyzing the effect of this distribution with respect to the production and flow pattern at equal distance between the perforations and the perforations part of the well father the toe. In the existing literature, less work has been done on the effect of DPD on horizontal well production in two-phase (air-water) environments.

One-phase flow has seen some useful studies, which many experts have participated in. The main variable that the study sought to establish their correlation includes friction (FR), PD, DPD and other variables of the study. For the assessment of the outcomes of the perforated horizontal wellbore performance, this study developed a sound semi-analytical approach. This model incorporates the PD in the wellbore and its influence upon flow, and production from the well. The model encompasses inflow PD through dimensions due to the in-flow, FR, and through ACC. Different gas-liquid velocity combinations were also considered in evaluating the SFP in the perforated horizontal wellbore. Negative influences on the oil production by the inertia effects in horizontal wells were replaced by the improvements of the PD through the SF.

2. Material and method

2.1. Experimental apparatus

Emulating the complicated flow in the horizontal wellbore was the goal of setting up the experimental setup Fig. 1 (a) and (b). The primary conduit, constructed of Perspex (an acrylic material), was 3 meters in length, had an inner diameter of 0.0254 meters, and had a perforated section with an inner diameter of 0.004 meters. The perforated horizontal pipe has 18 perforations cut into it at a phase angle of 180 degrees, all of which open vertically. With the use of the see through pipe, we were able to picture the flow patterns caused by the disparity in SVW and SVA. A total of 18 perforations are evenly distributed 35 cm from the heel of the pipe. An (ELP-USBGS800P03-MFV high-speed camera) Fig. 2, which has a frame rate of (640 fps), a pixel resolution of 320 × 240, and a recording range of 100-640 fps, depending on the flow patterns.

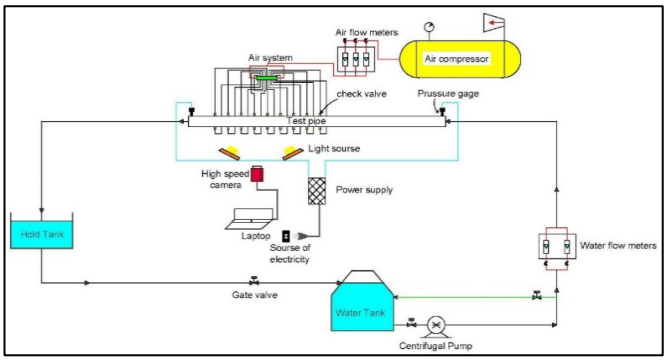

(a)

(b)

Fig. 1 A schematic illustrating the experimental apparatus.

SVW was injected into the main pipe using a centrifugal pump. The perforations in the pipe wall were filled with air using an electro-air compressor that injected an SVA. Two water flow meters were used to measure SVW rates ranging from 0.5 l/m to 4 l/m, 20 l/m to 110 l/m and three flow meters were used to measure SVA rates ranging from 1 l/m to 15 l/m, 3 l/m to 30 l/m and from 10 l/m to 100 l/m.

Fig. 2 High speed camera

Figure 3, show the test section, according to the research, different values of SVA ranged from 1 m/s to 4 m/s. In addition, different values of SVW ranged from 0.5 m/s to 3 m/s.

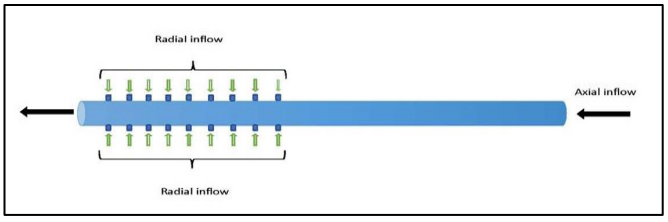

Fig. 3 An illustration of the test pipe schematic

3. Numerical procedures

3.1. Modeling assumptions

The Navier-Stokes equation is one example of a partial differential equation (PDE) that often represents the governing equations. Digital computers are unable to immediately answer these equations. The transformation of the governing equations into numerical equations involving just real values devoid of derivatives is of paramount importance. Converting partial differential equations to numerical equations is accomplished by numerical discretization. Number of numerical discretization techniques used include the finite volume method, finite element method, and finite difference approach. The accuracy of the finite volume technique is higher than that of the finite element method and the finite difference method, when contrasted with other approaches. And that's why the finite volume method of numerical discretization has become the gold standard Vresteeg [14], Muhmud [15] The physical model of the numerical simulation coincides with that in the experiment.

A horizontal perforated wellbore is simulated by three tests. in the scenarios of SVA these are 1.22, 2.52, and 1.22 m/s respectively and in the scenarios of SVW these are 1.68, 1.68, and 2.2 m/s. The present model solution is shown in Fig. 4 comprising the following parameters:

1. Newtonian liquid.
2. This is a turbulent, unsteady and incompressible flow.
3. According to numerical analysis two-dimensional geometry is maintained as in the experimental approach.
4. Air (SVA) and water (SVW) are the working fluids.
5. Properties of fluid flows remain constant.
6. A system is isothermal.

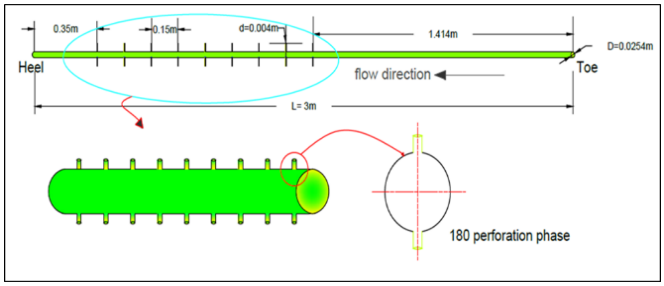

Fig. 4 Diagram illustrating the test section flow

3.2. CFD Ansys fluent

Utilizing the ANSYS Fluent 22 R1 program, a three-dimensional geometry resembling the experimental setup was generated. In order to examine the convergence behavior, many simulation runs were performed with total numbers of tetrahedral cells ranging from 1,116,042 to 4,079,683. Maximum skewness and minimum quality are the metrics used to evaluate mesh quality; values near 1 indicate poor maximum skewness and values around 0 indicate poor minimum quality. At these identical grid points, we also get the static pressure. To close the turbulence, 5-layer cells Realizable k-e model is prescribed next to the pipe wall because it will ensure that the right simulation will occur wall-wise. Figure 5 and Table 1 displays the numerical findings that were obtained. Specifically, the simulation used a grid of 2,601,065 components and 725,893 nodes.

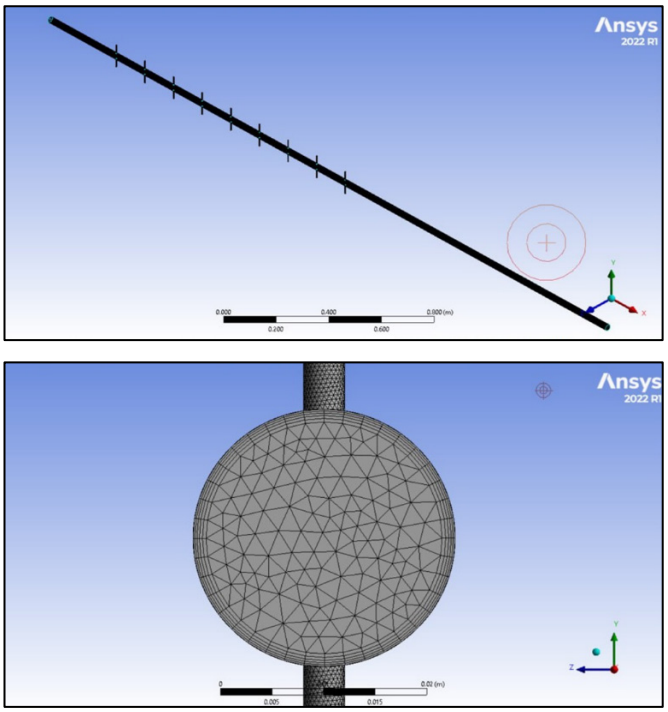

Fig. 5 Wellbore mesh model with horizontal perforations

Table 1. Grid independence at scenario 1 of SF (SVA = 1.68 m/s and SVW = 1.22 m/s)

Mesh	Nodes	Elements	Velocity (m/s)	Pressure (pa)
1	347,246	1,116,042	1.45179	1784.12
2	725,893	2,601,065	1.45826	1643.21
3	844,643	3,059,784	1.45944	1729.86
4	1,081,669	4,079,683	1.4608	1599.37

3.3. Initial and boundary conditions

1. Starting Conditions: At time $t = 0$ seconds, all the velocity components are suppressed ($t = t°$, $v = v°$). In addition, the VF of air is defined ($\alpha_a = 0$). The domain at first consists of water. The incoming air was applied at a fixed rate through the openings.
2. in Subdivisions of the Model: The numerical boundary conditions are stated in Table 2. These can be summarized as.

Table 2. Boundary condition.

Location	Boundary condition	Notes
At inlet	$u = U_{sw} = in$ and $\alpha_a = 0$ $v = U_{sa} = in_1, in_2, \ldots..,$ and in_{14} $\alpha_a = 1$	Velocity inlet (m/s) & VF for secondary phase
At outlet	$\frac{dU}{dx} = \frac{dV}{dy} = \frac{dW}{dz} = 0\ , p = 0$	Pressure outlet (pa)
At the wall	$U = V = W = 0$	No-slip condition

3.4. The two-phase flow models

In the commercially available Fluent 22 R1 CFD software, a homogeneous model is utilized to represent the two-phase flow behavior of gas-liquid flow pattern. This is accomplished through the utilization of the Volume of Fluid (VOF) technique. Assuming that the local velocity and pressure do not change across the different stages, this model provides an explanation. On the subject of three-dimensional geometry, this model makes use of the Navier-Stokes equations in order to do an analysis of turbulent, unsteady state, and mixing flows. For the purpose of resolving turbulent flows, the Realizable approach is utilized in conjunction with the k-ε model. This technique is based on the viscosity of the flow patterns and the wall function. When there is no interpenetration of fluids or phases, VOF can be either a steady or a transient formulation. A steady formulation is the more common type. Following the completion of the entire numerical computation, a total volume fraction of one is obtained for each control volume. Each location's volume proportion of gas and liquid is something that we are aware of. In light of this, the variables and characteristics that are included within a certain cell either reflect all phases or only one of them, depending on the values of VF. When the VF of the q_{th} fluid in the cell is designated as α_q, there are three unique conditions that apply [16]. These conditions are described using the same language.

$\alpha_q = 0$: The q_{th} fluid cell is devoid of any contents.
$\alpha_q = 1$: With the q_{th} fluid, the cell is filled.
$0 < \alpha_q < 1$: The q_{th} fluid's interaction with other accessible fluids is a part of the cell.

The following is the procedure for estimating the mixture's dynamic viscosity μ_m and density ρ_m in the VOF model:

$$\rho_m = \rho_g\, \alpha_q + \rho_l \left(1 - \alpha_q\right) \tag{1}$$

$$\mu_m = \mu_g \alpha_q + \mu_l \left(1 - \alpha_q\right) \tag{2}$$

Where the liquid phase is denoted by the subscript (l), and the gas phase by the subscript (g).

3.5. Governing equations

Any flow problem's numerical simulation can be simplified to the solving of the basic equations relevant to the turbulence, mass and momentum explanation. Also, the VF conservation equation for each phase in the domain. Basic geophysical equations for each phase are given below:

3.5.1. Mass conservation

Get the VF of one or more phases by solving the continuity equation. This equation is stated in the following form for the q_{th}phase [17].

$$\frac{\partial}{\partial t}(\alpha) + \nabla.\left(\alpha \overrightarrow{V_m}\right) = 0 \tag{3}$$

According to [14], [18] the equation that describes the continuity of the mixture occurs when it is in an unstable situation.

$$\frac{\partial}{\partial t}(\rho_m) + \nabla.\left(\rho_m \overrightarrow{V_m}\right) = 0 \tag{4}$$

The mass equation in three dimensions:

$$\frac{\partial \rho_m}{\partial \mathrm{t}} + \frac{\partial(\rho_m U_m)}{\partial x} + \frac{\partial(\rho_m V_m)}{\partial y} + \frac{\partial(\rho_m W_m)}{\partial z} = 0 \tag{5}$$

3.5.2. Conservation of momentum

The VF of all phases, as given below [18], [19], provide the basis of the momentum equation through the characteristics ρ_m and μ_m.

$$\frac{d}{dt}(\rho_m \overrightarrow{V_m}) + \nabla \cdot (\rho_m \overrightarrow{V_m}\,\overrightarrow{V_m}) = -\nabla P + \rho_m \vec{g} + \nabla \cdot [\mu_m (\nabla \overrightarrow{V_m} + \nabla \overrightarrow{V_m}^T)] + \vec{F} \quad (6)$$

Where:
$\left[\mu_m (\nabla \overrightarrow{V_m} + \nabla \overrightarrow{V_m}^T)\right]$: Is the viscous stress tensor
$\overrightarrow{F}$: Is a continuum surface force vector.

3.6. Total pressure drops (TPD)

There are four parts to the PD over a horizontally perforated wellbore: Friction pressure drop (FRPD/ΔP_{wall}), Acceleration pressure drop (ACCPD/ΔP_{acc}), Perforation roughness pressure drop (PRPD/ΔP_{perf}), and Mixing pressure drop (MPD/ΔP_{mix}). All these parameters are measured by Pascal (Pa).

$$\Delta P = \Delta P_{wall} + \Delta P_{acc} + \Delta P_{perf} + \Delta P_{mix} \quad (7)$$

Thus, as demonstrated in [20], [21], the four distinct PD of a TFF were computed by substituting the laws of a single-phase flow with their corresponding variables of a TFF.

$$\Delta P_{wall} = \frac{f_o \rho_m U_m^2 \Delta x}{2D} \quad (8)$$

$$\Delta P_{acc} = 2\rho_m U_m \frac{q_p}{A} \rho_m \left(\frac{q_p}{A}\right)^2 \quad (9)$$

$$\Delta P_{perf} = \frac{f_p U_m^2 \Delta x}{2D} \quad (10)$$

$$\Delta P_{mix} = ((\Delta P_{perf} - 0.031 Re_{2ph} \xi p(\xi p \le 0.1)\, 760\, (\xi p > 0.1)) \quad (11)$$

$$f_p = 4D \frac{q_l}{q} + 2\frac{D}{n}\left(\frac{q_l}{q}\right)^2 \quad (12)$$

Where:
ξ_p: the ratio of inflow rate through one perforation to main flowrate, and

$$\xi_p = \frac{q_p}{q} \quad (13)$$

q_l: inflow rate per unit length (m^3 / s /m), Where:

$$q_l = \frac{n v_p \pi d^2}{4} \quad (14)$$

q_f: inflow rate through each perforation (m^3/s).
q: main flow rate (m^3/s).
f_p: equivalent friction factor due to influx
N: perforation density (m^{-1}).

According to the work of [21], the overall effective friction factor is equal to the sum of the perforation friction factor and the wall friction factor.

$$f = f_o + f_p \quad (15)$$

Using equation (15) the sum of the friction PD across the wall and the PD across the perforation is the total friction pressure drop (TFPD).

4. Result and discussion

4.1. Simulation of SFP in perforated horizontal wellbore

The formation of a SFP occurs when we raise the AFR and average WFR. Figures 6 to 8 illustrate the behavior of the SFP in a horizontally perforated well across three distinct scenarios, starting from the onset of bubble formation at 0.09 seconds and culminating in the formation of slugs at full time. In the first scenario, as shown in Fig. 6, the SV of the air is 1.68 m/s, meanwhile the SV of the water is 1.22 m/s. The results demonstrate that large bubbles (EB) generate within the well's higher regions differentiated from one another by fluid-filled areas, while small bubbles in the fluid appear on both sides when the slug ascends through the lower perforations. The results demonstrate that bubbles start to generate in the 1st perforation because the SV of air is adequate to cause the bubbles to merge and coalesce into larger bubbles.

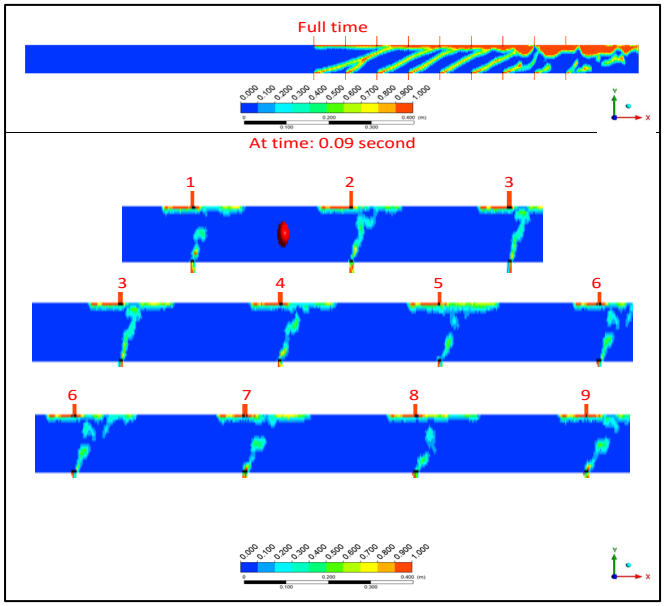

Fig. 6 The behavior of the SFP for a horizontally perforated well (scenario 1)

The elongated bubbles (EBS) are largest after the fourth perforation due to the air flowing through more perforations. The scale reaches its peak at 1.008 seconds, which corresponds to scenario 1. In the second scenario, the SV of water increases to 2.52 m/s, meanwhile the SV of air does not change (1.68). It can be seen in Fig. 7 that this scenario differs from the first in that the air-water arrangement is different in fluid flow. The increase in fluid flow caused an increase in fluid content and a decrease in porosity fraction; therefore, the size of the EB appears smaller compared to the first scenario. In scenario 2, the scale measures 1.008 seconds. In the last scenario, the SV of air increases to 2.2 m/s, meanwhile the SV of water does not change (1.22). As the air SV increases, massive bubbles form as air fills a wider region along the wellbore. The results indicate that there is no important difference between the first and last scenarios with

constant SVW and different SVA, as the increase in SVA does not significantly alter the air-water configuration or lead to an SVW. The time is 1.008 seconds (scenario 3), as shown in Fig. 8.

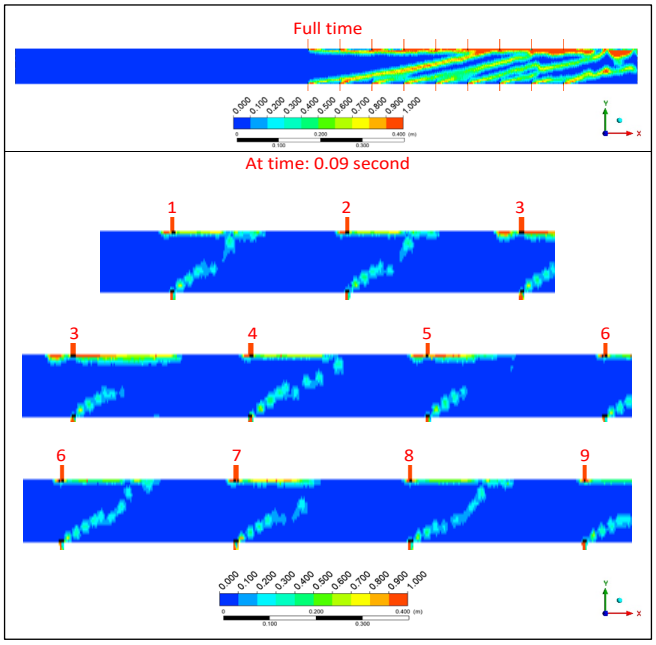

Fig. 7 The behavior of the SFP for a horizontally perforated well (scenario 2)

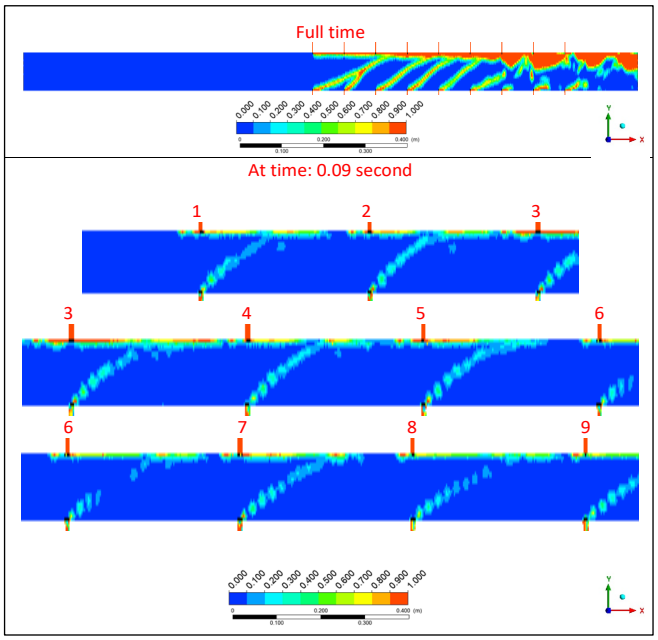

Fig. 8 The behavior of the SFP for a horizontally perforated well (scenario 3)

4.2. Slug flow behavior

The SF behavior is similar for all the perforations and the values of the SVA = 1:68 m/s, SVW = 1:22 m/s as shown in Fig. 9. After the wellbore with water is completely packed, and the perforation holes are kept open; air starts to be introduced slowly through the perforations and bubbles are introduced low. The air enclosed in the water jetting towards the upper region of the well due to buoyancy starts from the moment air is introduced from 0.09 seconds to 0.25 seconds, the time when the air is exhausted. Since air bubbles had been building up in the upper wellbore of the lower as well as the upper perforations, it means air mass formation but should begin within the range of timing 0.5 to 0.75 seconds where the long bubbles began. That is the scenario where the long bubbles were said to have started increasing their volumes at the duration of 0.75 seconds even when the thickness of the surrounding liquid was reduced. Long bubbles are defined as those which comprise of thick liquid slugs having small air bubbles distributed within that thick liquid. In reviewing the liquid slug flow, the confined liquid slug is small because there is an air phase that is in continuous flow along the horizontal wellbore which captures more air volume causing the range in liquid slug that is observed in the forward-looking region of about looking at 1.008 seconds to be the least. The slug unit functions at a condition of quasi equilibrium.

One variation on the slug flow pattern is presented in Fig. 10 where the air and water S.V. are equal to 1.68 m/s and 2.52 m/s, respectively. The conclusions present a behavior that is closest to the first scenario. On the other hand, with the increase in the inflow water rate, the EBS are expected to change in extent in that they will be shorter than in the first scenario but also more convergent. This increased the liquid film and decreased the VF at the same time. Therefore, liquid slugs and EBS are created. In addition, by increasing water SV in which the AXF is increased, the PD increases more due to higher height of water column in the well bore and higher volume of water in contact with upper wall of the well bore as was a scenario of [22], hence smaller than other scenarios of EBS was expected. Fig. 11 shows a SF regime under SVA of 2.2 m/s and SVW of 1.22 m/s. The bubbles that are coming from the bottom perforations are observed to be many and bigger than previous ones unapologetically air bubbles which heightened from the bottom perforations more and larger in size than previous ones, which is due to more air flow. In addition, when the number of the EBS increases. An increase in SVA results in a corresponding increase in the air slug length. [23] reached a similar conclusion. Figures 9, 10 and 11 present the CFD and experimental data for three scenarios of SF. There was a good compactness; notably, these scenarios indicate that the numerical results are well supported by the real experimental data.

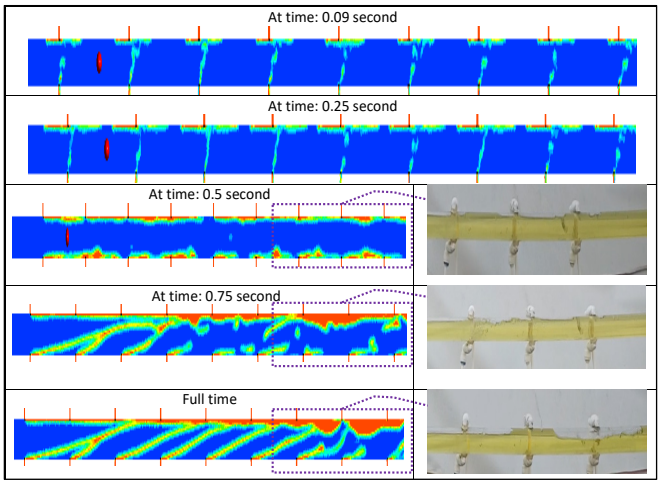

Fig. 9 Comparing and analyzing experimental and numerical results scenario (1)

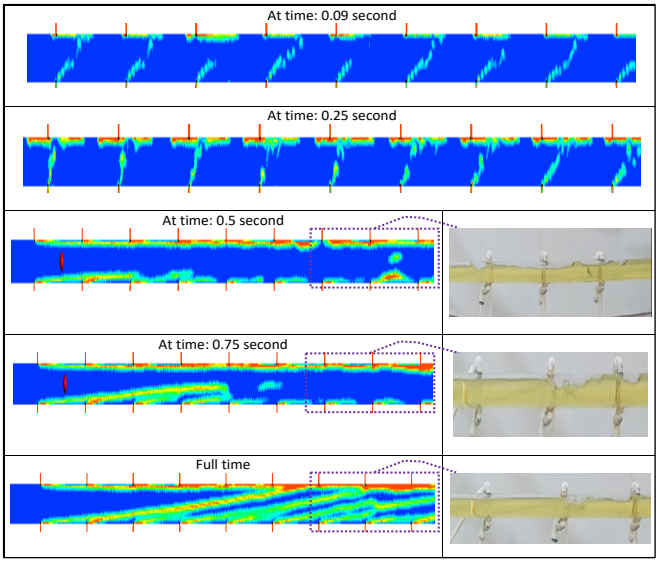

Fig. 10 Comparing and analyzing experimental and numerical results scenario (2)

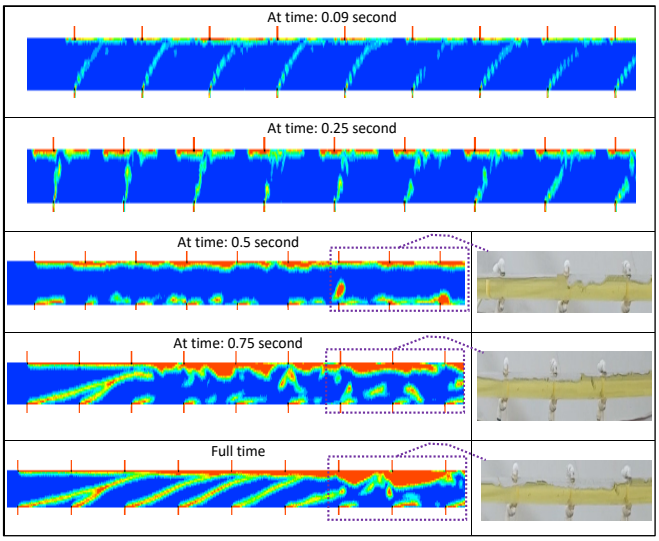

Fig. 11 Comparing and analyzing experimental and numerical results scenario (3).

4.3. Pressure drops in slug flow

The indicator of TPD in the horizontal wellbore pattern occurs in all three scenarios as seen in Fig. 12. The data indicated PD fluctuations; however, the PD as the length of the horizontal pipe without perforation is raised appeared to increase in a linear manner. Air entering through the horizontal perforations in the wellbore continued to cause an increase in PD in the main wellbore. The results suggest that where the perforation is made reduces the frictional drag because it has an inflow of air via the perforations. PD distribution pattern in horizontal wellbore and it was shown that there was an increase in pressure wavy fluctuations on the horizontal pipe perforated when subjected to a PD. Owing to the inward interring of air through the perforations in the area with perforations in the horizontal wellbore. Which resulted in an unrestrained increase in the mixture velocity in a main wellbore.

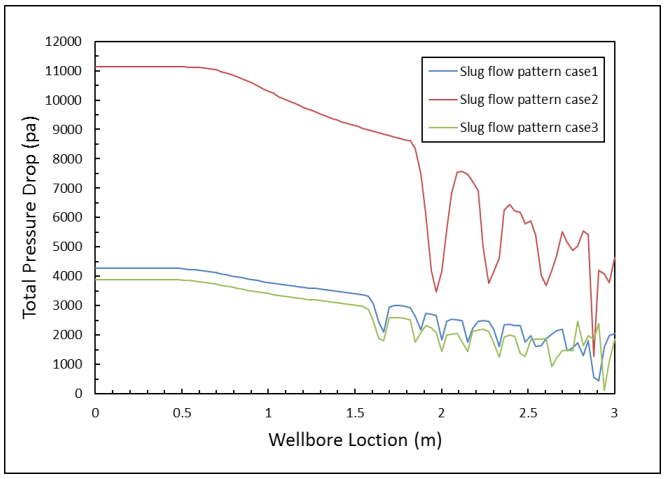

Fig. 12 TPD distribution throughout the horizontal wellbore

The results indicate that at the level of the perforations the frictional drag reduces owing to the admission of air through the perforations, there was also the decrease of the FRPD in this zone along with reduction in the mixture's density, the FRPD in this region, as do the mixing and ACCPD. Consequently, the TPD, but such phenomena occur in every scenario, where the heel-end of the well is concerned considering the increase in the mixture velocity along with the lowering of the VF in this area. In the first scenario, portrays the amount of TPD down the horizontal wellbore during the first scenario. The results show a marked PD on location 1.41m to the end of the wellbore due to more accumulation of air in those places. Pressure assisted flow where in the second scenario, only the SVW was increased with respect to the previous instances and it was observed that the outcome was significantly affected when this parameter was changed.

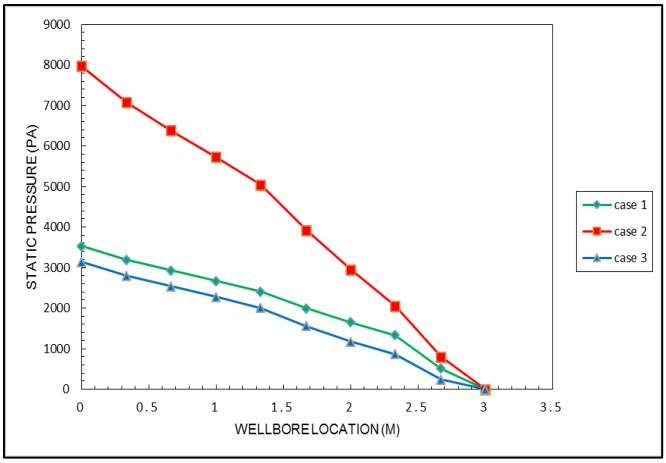

Fig. 13 SPD distribution throughout the horizontal wellbore

The last scenario occurs when the RDF (SVA) 2.2 m/s is increased, while the AXF where the casing (SVW) is held constant at 1.22 m/s. This is evident in the last scenario where the increase in the velocity through the perforations does not have a significant influence on the PD with only a small PD increase compared to the second scenario. The decrease in PD variation stabilizes across the horizontal wellbore as a result of enhanced movement of air due to the improved air flow from the reservoir via the perforations. Figure 13 depicts the average SPD profile along the horizontal wellbore for all

the three scenarios. Figure 14 shows the SPD contours. The highest SPD level was observed in the regions close to the entrance of the horizontal wellbore due to very high density and viscosity values. SPD measured within the wellbore decreases in a downward direction and finally reaches a lowest off PD towards the bottom region of the wellbore. This PD increases steadily as the SVW of the fluid volume in the moderation increases or rather the level of SVW, as well as the SVA of fluid volume in the vessel, SVA, increases. Its SPD as shown in the last scenario study does not affect them as a lower VF compared to water does not exert much pressure. The mixture only shows slight changes in density and viscosity; however, the SPD remains comparable to the first scenario.

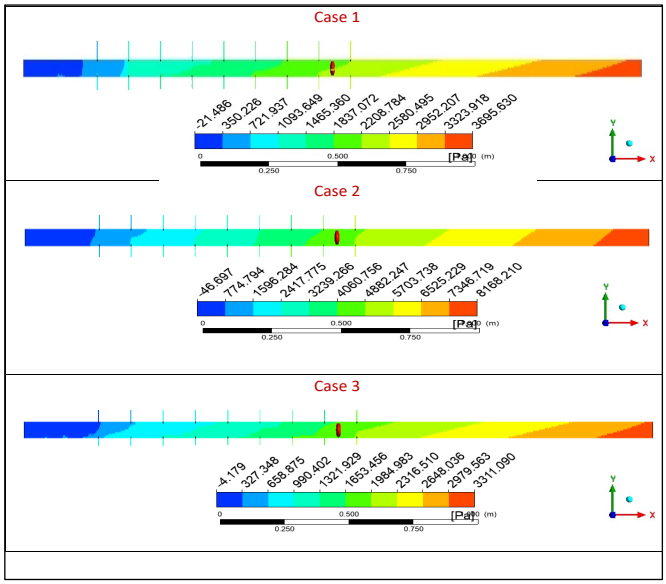

Fig. 14 SPD distribution throughout the horizontal wellbore

4.4. Productivity in horizontal wellbore

Figure 15 compares the flow rate in three separate scenarios along a horizontal wellbore at a time in three separate scenarios. It can be observed that because of a continuous inflow of fluids into the wellbore through the perforation from the reservoir, the flow rates seem to increase from the toe of the wellbore to the heel of the horizontal wellbore. It is evident from the results that high values of the SVW results in the maximum production since it enhances the withdrawal of more water from the mother pipe. A significant drop in the rate of fluid mass flow is however observed at the point of perforations, where SVW scenarios and SVA is initiated. This difference is owing to the fact that air is drawn faster than water, and thus, a greater air flow leads to a faster flow rate. However, after the perforation location has been attained, the flow rate does not decrease once again. In the last scenario, the SVA has been increased to 2.2 m/s but the SVW remains constant at 1.22 m/s.

The increase in productivity is however not as much as in comparison with the second scenario. Flows through the inlet circular perforations decrease with the increasing perforation's diameter which differ from the second scenario where volume of water in taken from the current. In this scenario, the rate of flow at the position of the perforations has been improved by virtue of the fact that the radial vector velocity entering through the perforations is more than the AXF. Fluids can be transported with a higher flow rate because both substantial AXF and RDF contribute to higher velocity.

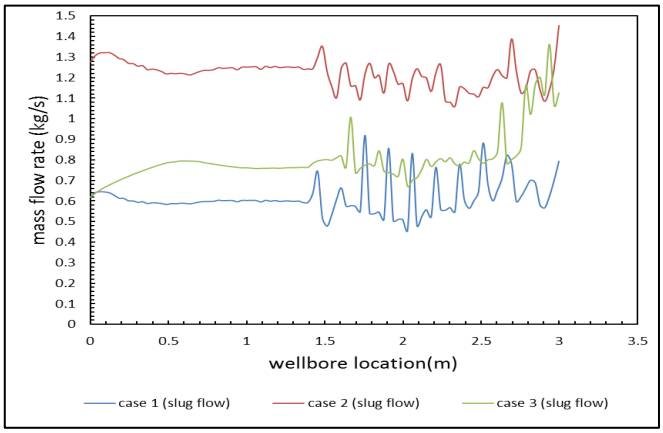

Fig. 15 Horizontal wellbore productivity

4.5. The conduct of the MSV in the perforated horizontal wellbore

Figure 16 presents the results regarding the velocity of the (MSV) in a horizontal perforated well. Other than this, there was the velocity fluctuation in the perforated section of the horizontal well, particularly because of the radial air phase momentum. It was noted that the velocity in the non-perforated part behaves more or less in a straight highland with minimal changes. No matter, in the back non-perforated portion, there was a smooth flow movement. Because there was water and only one phase. However, when air that is introduced from the first perforations of the perforated part, the fluctuation behavior in the radial air phase is lower than the behavior in the last part of the perforated part. This is due to high velocity and high volume of the radial air phase in the perforated part, while the end scenario more than the first and second scenarios caused the fluctuations trains to grow more than the first and second scenario.

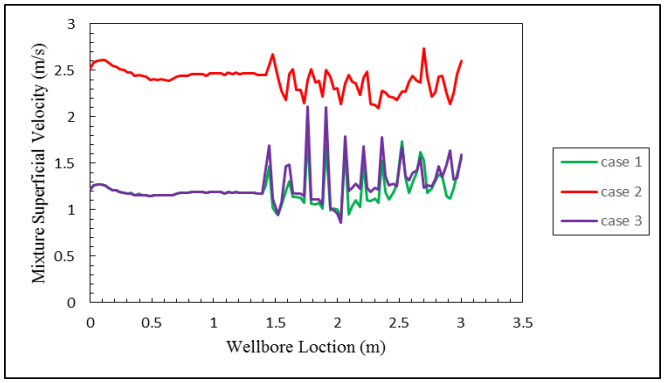

Fig. 16 the MSV distribution along the length of horizontal wellbore

4.6. Distribution of volume fraction

The important design parameters although revolved around design processes of the two phase pipelines and their associated appliances, the VF and LH of a SF are significant [24]. The behavior of the VF in the perforated horizontal was mentioned while for the explanatory understanding, the behavior and the drift in the perforated part was derived of the RDF, the hollow portion while it was steady in the non-perforated portion.

It was observed that the VF values were higher for an increasing SVA but at that point when the final SVW was lower than the last SVA, SVA, thus like most of MSV and contrary to the whole PD. The VF mechanism can also be regarded as foam volumes within the perforated pipe. In others, it was taken as the volume of pneumatic phase along the perforated horizontal tube thus, was strategically incorporated into the schematic presentation of it, as it could be noted in Figs. 17 (scenario 1), 18 (scenario 2), and 19 (scenario 3). These figures represent changes of the VF in the horizontal wellbore at certain given instances of time (0.2, 0.5, 0.7 and full time)/second with regards to three scenarios, the data demonstrated how the VF varied with the variations in the TFF rates and also when the SF developed and moved in the wellbore at various times.

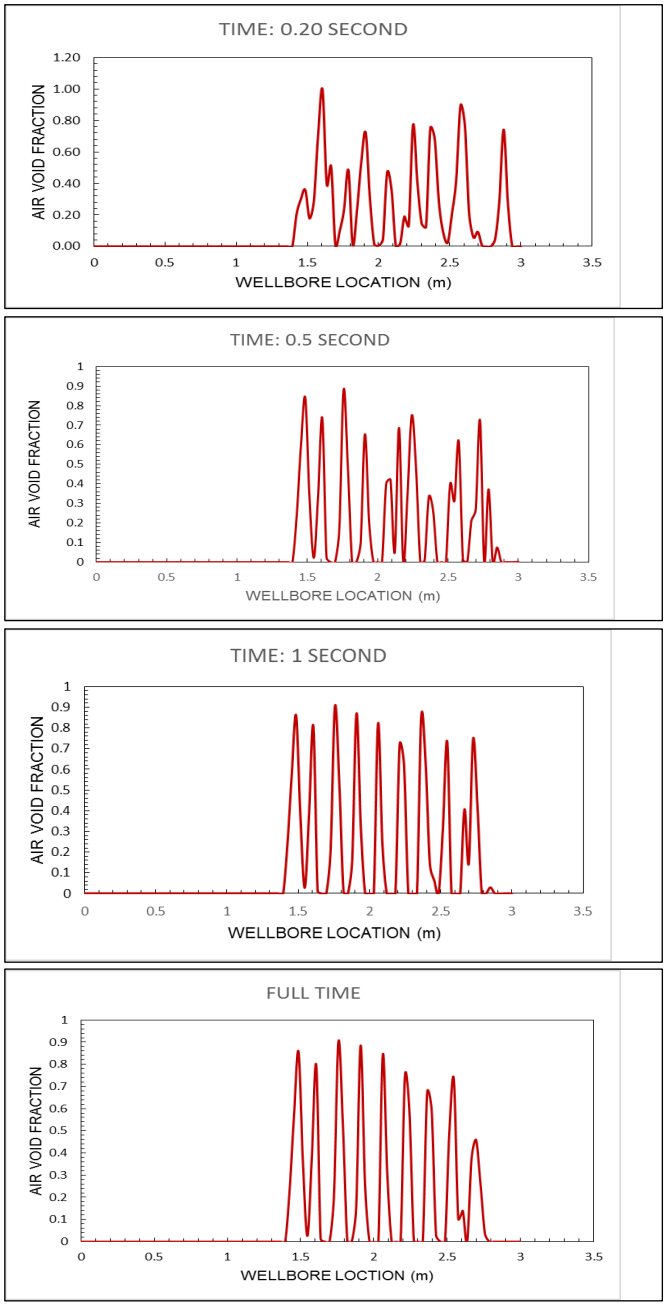

Fig. 17 The VF distribution along the length of horizontal wellbore (first scenario)

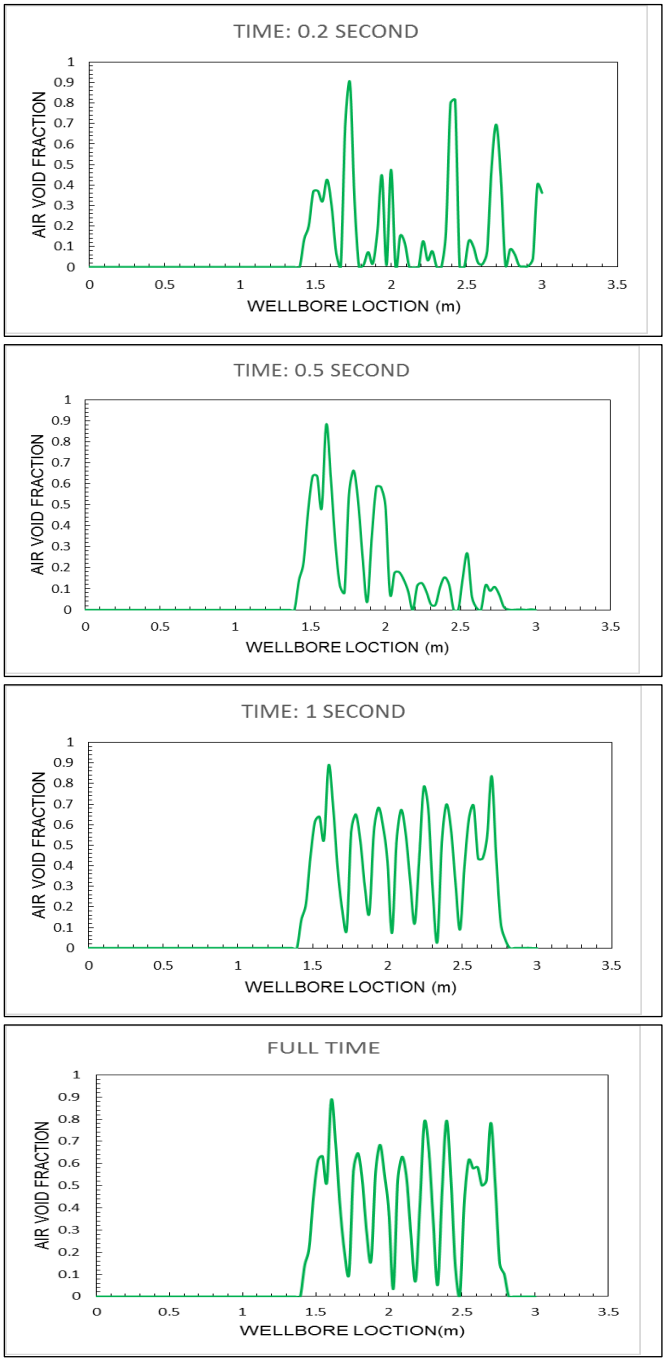

Fig. 18 The VF distribution along the length of horizontal wellbore (second scenario)

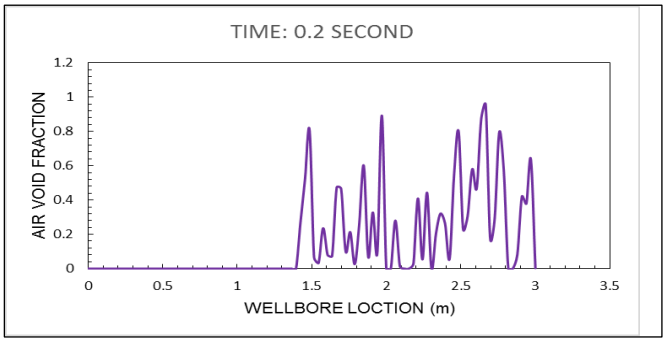

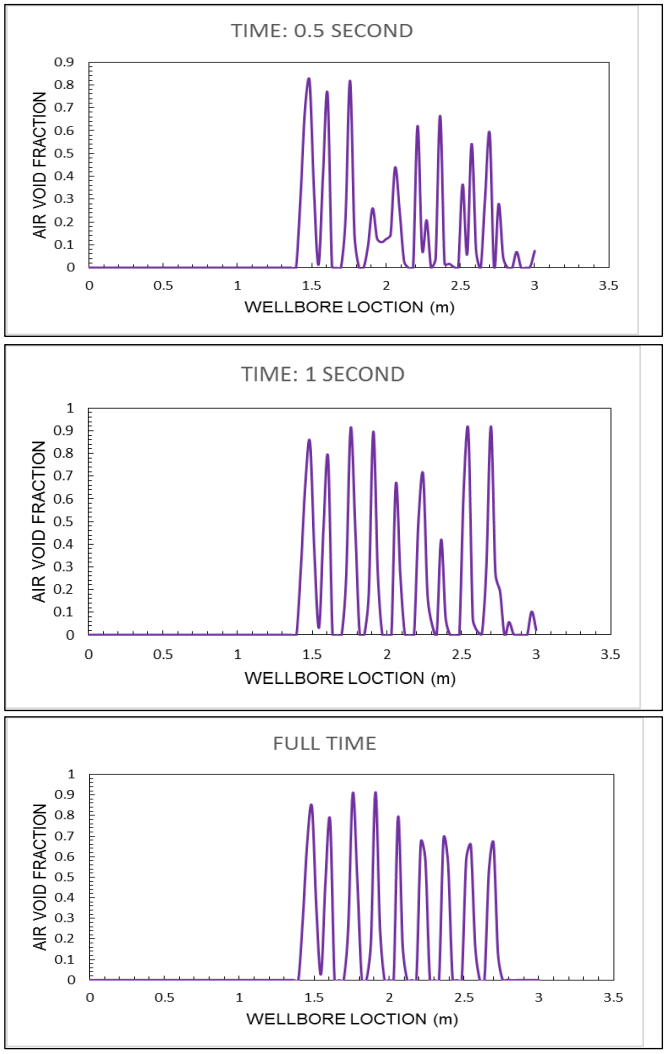

Fig. 19 The VF distribution along the length of horizontal wellbore (third scenario)

4.7. Flow pattern map of two-phase flow

The TFFP and The SF used in this study at different gas and liquid SVA and SVW are shown in Fig. 18. While the red velocity values are solely obtained by experimental research, the green ones come from both numerical and experimental Analysis. This study's conclusions on the TFFP map in horizontal wellbore configurations are in good agreement with those of [25].

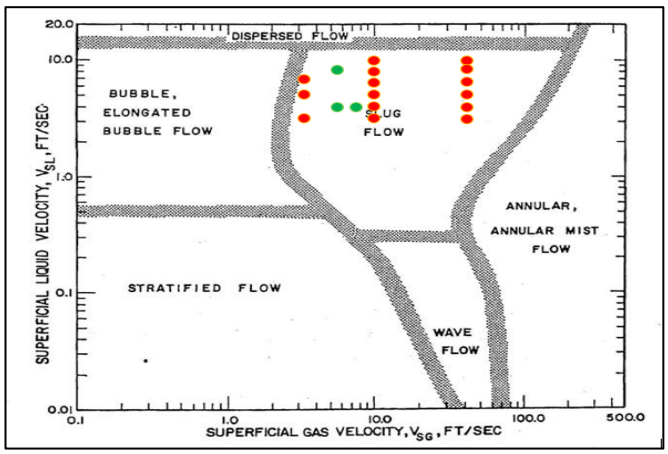

Fig. 20 Schematic representation of the configuration of two-dimensional horizontal flow in the presence of stratified two phases.

5. Conclusions

The SFP in the horizontal screen wellbore was studied through a purely numerical approach as well as through experimental investigation. The decisions that were down:

1. This paper performs numerical modeling of slug turbulent two-phase air-water flow in a horizontal perforated wellbore using ANSYS FLUENT 22R1 VOF approach and Realizable (k-ε) model with unsteady state.
2. Considering the way that the existing formulation may be quite difficult because of the fine grids and the time of the computation necessary, it appears that the simulation of SFP can be carried out very well by use of CFD.
3. It looks like the experimental and computational exploration of the schematized two-dimensional slug motion has confirmed its belonging to the Mandhane's slug map and matched.
4. Air slugs increased in length with increasing SVA, while liquid slugs increased in number with increasing SVW.
5. As far as SVA is concerned that is PD linear approximately. Combinatorial optimization is the location and the PD. As long as SVW and SVA are continuously increasing maximum.
6. The improvement in productivity increased considerably with the increase in SVW when compared to the first scenario while in the third scenario, the increase in productivity was less than the second scenario when considering the SVA. So, in this case, it is understood that the higher the SVW, the higher the productivity.
7. There exists a reasonable correlation between the patterns of slug flow seen in the experiments and the numerical calculations.

References

[1] H.-G. Kim and S.-M. Kim, "Experimental investigation of flow and pressure drop characteristics of air-oil slug flow in a horizontal tube," International Journal of Heat and Mass Transfer, vol. 183, p. 122063, 2022. https://doi.org/10.1016/j.ijheatmasstransfer.2021.122063

[2] H. Müller-Steinhagen and K. Heck, "A simple friction pressure drop correlation for two-phase flow in pipes," Chemical Engineering and Processing: Process Intensification, vol. 20, pp. 297-308, 1986. https://doi.org/10.1016/0255-2701(86)80008-3

[3] B. A. Shannak, "Frictional pressure drop of gas liquid two-phase flow in pipes," Nuclear engineering and design, vol. 238, pp. 3277-3284, 2008. https://doi.org/10.1016/j.nucengdes.2008.08.015

[4] Y. Taitel and D. Barnea, "Two-phase slug flow," Advances in heat transfer, vol. 20, pp. 83-132, 1990. https://doi.org/10.1016/S0065-2717(08)70026-1

[5] G. H. Abdul-Majeed, "Liquid slug holdup in horizontal and slightly inclined two-phase slug flow," Journal of Petroleum Science and Engineering, vol. 27, pp. 27-32, 2000. https://doi.org/10.1016/S0920-4105(99)00056-X

[6] T. Yildiz, "Inflow performance relationship for perforated horizontal wells," SPE Oklahoma City Oil and Gas Symposium/Production and Operations Symposium, pp. SPE-67233-MS, 2001. https://doi.org/10.2118/67233-MS

[7] J. Thaker and J. Banerjee, "Characterization of two-phase slug flow sub-regimes using flow visualization," Journal of Petroleum Science and Engineering, vol. 135, pp. 561-576, 2015. https://doi.org/10.1016/j.petrol.2015.10.018

[8] M. A. Abdulwahid, H. J. Kareem, and M. A. Almudhaffar, "Numerical analysis of two phase flow patterns in vertical and horizontal pipes," WSEAS Transactions on Fluid Mechanics, vol. 12, pp. 131-140, 2017.
[9] M. Azadi, S. M. Aminossadati, and Z. Chen, "Development of an integrated reservoir-wellbore model to examine the hydrodynamic behaviour of perforated pipes," Journal of Petroleum Science and Engineering, vol. 156, pp. 269-281, 2017. https://doi.org/10.1016/j.petrol.2017.05.027
[10] A. E. Dukler and M. G. Hubbard, "A model for gas-liquid slug flow in horizontal and near horizontal tubes," Industrial & Engineering Chemistry Fundamentals, vol. 14, pp. 337-347, 1975. https://doi.org/10.1021/i160056a011
[11] L. Hua, L. Yan, P. Xiaodong, L. Xindong, and W. Laichao, "Pressure drop calculation models of wellbore fluid in perforated completion horizontal wells," IJHT, International Journal of Heat and Technology, vol. 34, pp. 65-72, 2016. https://doi.org/10.18280/ijht.340110
[12] J. Wen, M. Yang, W. Qi, J. Wang, Q. Yuan, and W. Luo, "Experimental analysis and numerical simulation of variable mass flow in horizontal wellbore," International Journal of Heat & Technology, vol. 36, pp. 309-318, 2018. https://doi.org/10.18280/ijht.360141
[13] M. J. Landman, "Analytic modelling of selectively perforated horizontal wells," Journal of Petroleum Science and Engineering, vol. 10, pp. 179-188, 1994. https://doi.org/10.1016/0920-4105(94)90079-5
[14] H. K. Versteeg, An introduction to computational fluid dynamics the finite volume method, 2/E: Pearson Education India, ISBN: 978-0-13-127498-3 , 2007.
[15] H. Ben Mahmud, Multiphase transient flow in pipes, Curtin University, ISBN 978-3-7258-1131-1, 2012.
[16] W. Yuan, S. Liu, S. Li, T. Tao, and K. Xin, "Numerical simulation of bubble motion in horizontal reducer pipelines," Engineering Applications of Computational Fluid Mechanics, vol. 5, pp. 517-529, 2011. https://doi.org/10.1080/19942060.2011.11015391
[17] G. N. Patel, CFD Simulation of Two-phase and Three-phase Flows in Internal-loop Airlift, Lappeenranta University of Technology, ISBN 53850, 2010. https://urn.fi/URN:NBN:fi-fe201009062401
[18] S. Y. Razavi and M. M. Namin, "Numerical model of slug development on horizontal two-phase flow," in Proceedings of The International Conference on Recent Trends in Transportation, Environmental and Civil Engineering, pp. 53-57, 2011.
[19] V. Ranade, "Computational flow modelling for chemical reactor engineering," Academic press London NW1, 2002. ISBN 0-12-576960-1.
[20] Z. Su and J. Gudmundsson, "Friction factor of perforation roughness in pipes," in SPE Annual Technical Conference and Exhibition, p. SPE-26521-MS, 1993. https://doi.org/10.2118/26521-MS
[21] H. Asheim, J. Kolnes, and P. Oudeman, "A flow resistance correlation for completed wellbore," Journal of Petroleum Science and Engineering, vol. 8, pp. 97-104, 1992. https://doi.org/10.1016/0920-4105(92)90048-6
[22] Z. Liu, R. Liao, W. Luo, J. X. Ribeiro, and Y. Su, "Friction pressure drop model of gas-liquid two-phase flow in an inclined pipe with high gas and liquid velocities," AIP Advances, vol. 9, 2019. https://doi.org/10.1063/1.5093219
[23] M. Andrianto, A. Widyaparaga, and O. Dinaryanto, "CFD Studies on the gas-liquid plug two-phase flow in a horizontal pipe," Journal of Petroleum Science and Engineering, vol. 147, pp. 779-787, 2016. https://doi.org/10.1016/j.petrol.2016.09.019
[24] Z. I. Al-Hashimy, H. H. Al-Kayiem, R. W. Time, and Z. K. Kadhim, "Numerical characterisation of slug flow in horizontal air/water pipe flow," International Journal of Computational Methods and Experimental Measurements, vol. 4, pp. 114-130, 2016. https://doi.org/10.2495/CMEM-V4-N2-114-130
[25] J. Mandhane, G. Gregory, and K. Aziz, "A flow pattern map for gas—liquid flow in horizontal pipes," International journal of multiphase flow, vol. 1, pp. 537-553, 1974. https://doi.org/10.1016/0301-9322(74)90006-8